European Journal of Nuclear Medicine and Molecular Imaging (2020) 47:1198–1208
https://doi.org/10.1007/s00259-020-04682-5

ORIGINAL ARTICLE

Influx rate constant of ^{18}F-FDG increases in metastatic lymph nodes of non-small cell lung cancer patients

Min Yang[1,2] · Zhong Lin[3] · Zeqing Xu[4] · Dan Li[1,2] · Weize Lv[3] · Shuai Yang[3] · Ye Liu[5] · Ying Cao[6] · Qingdong Cao[7] · Hongjun Jin[1,2]

Received: 31 August 2019 / Accepted: 2 January 2020 / Published online: 23 January 2020

Abstract

Purpose Primary tumor (PT) and metastatic lymph node (MLN) status have a great influence on diagnosis and treatment of lung cancer. Our main purpose was to investigate the imaging characteristics of PT or MLN by applying the ^{18}F-FDG PET dynamic modeling approach for non-small cell lung cancer (NSCLC).

Methods Dynamic ^{18}F-FDG PET scans were performed for 76 lung cancer patients, and 62 NSCLC cases were finally included in this study: 37 with newly diagnosed early and locally advanced lung cancer without distant metastases (group M0) and 25 metastatic lung cancer (group M1). Patlak graphic analysis (K_i calculation) based on the dynamic modeling and SUV analysis from conventional static data were performed.

Results For PT, both K_i^{PT} (0.050 ± 0.005 vs 0.026 ± 0.004 min^{-1}, $p < 0.001$) and SUV^{PT} (8.41 ± 0.64 vs 5.23 ± 0.73, $p < 0.01$) showed significant higher values in group M1 than M0. For MLN, K_i^{MLN} showed significant higher values in M1 than M0 (0.033 ± 0.005 vs 0.016 ± 0.003 min^{-1}, $p < 0.01$), while no significant differences were found for SUV^{MLN} between M0 and M1 (4.22 ± 0.49 vs 5.57 ± 0.59, $p > 0.05$). Both SUV^{PT} and K_i^{PT} showed significant high values in squamous cell carcinoma than adenocarcinoma, but neither SUV^{PT} nor K_i^{PT} showed significant differences between EGFR mutants versus wild types. The overall Spearman analysis for SUV and K_i from different groups showed variable correlation ($r = 0.46$–0.94).

Conclusion The dynamic modeling for MLN (K_i^{MLN}) showed more sensitive than the static analysis (SUV) to detect metastatic lymph nodes in NSCLC, although both methods were sensitive for PT. This methodology of non-invasive imaging may become an important tool to evaluate MLN and PT status for patients who cannot undergo histological examination.

Clinical trial registration The clinical trial registration number is NCT03679936 (http://www.clinicaltrials.gov/).

Keywords Non-small cell lung cancer · ^{18}F-FDG · Dynamic PET/CT · Patlak · Metastatic lymph nodes

Min Yang, Zhong Lin and Zeqing Xu contributed equally to this work.

This article is part of the Topical Collection on Oncology – Chest.

Electronic supplementary material The online version of this article (https://doi.org/10.1007/s00259-020-04682-5) contains supplementary material, which is available to authorized users.

✉ Qingdong Cao
15013813866@163.com

✉ Hongjun Jin
jinhj3@mail.sysu.edu.cn

[1] Guangdong Provincial Key Laboratory of Biomedical Imaging and Guangdong Provincial Engineering Research Center of Molecular Imaging, The Fifth Affiliated Hospital, Sun Yat-sen University, Zhuhai 519000, Guangdong Province, China

[2] Center of Molecular Imaging, The Fifth Affiliated Hospital, Sun Yat-sen University, Zhuhai 519000, Guangdong Province, China

[3] Center of Oncology, The Fifth Affiliated Hospital, Sun Yat-sen University, Zhuhai 519000, Guangdong Province, China

[4] Department of Nuclear Medicine, The Fifth Affiliated Hospital, Sun Yat-sen University, Zhuhai 519000, Guangdong Province, China

[5] Department of Pathology, The Fifth Affiliated Hospital, Sun Yat-sen University, Zhuhai 519000, Guangdong Province, China

[6] The First Medical Center of PLA General Hospital, Beijing 100853, China

[7] Department of Cardiothoracic Surgery, The Fifth Affiliated Hospital, Sun Yat-sen University, Zhuhai 519000, Guangdong Province, China

Introduction

Lung cancer is the most common cancer and the leading cause of cancer-related death worldwide [1]. There are two major types of lung cancer, small cell lung cancer (SCLC), and non-small cell lung cancer (NSCLC). Roughly 85% of diagnosed lung cancers are NSCLC. Adenocarcinoma (AC) and squamous cell carcinoma (SCC) account for the majority of NSCLC [2]. In clinical practice, primary tumor (PT) and mediastinal metastatic lymph node (MLN) status have a great influence on treatment choice and disease prognosis. Computed tomography (CT) and mediastinoscopy are routinely applied for preoperatively diagnosing mediastinal MLN metastases in resectable lung cancers. The determination of the optimal criterion for a CT diagnosis is purely based on node size, which may cause false positive or negative diagnosis. It can thus be considered that functional imaging method, such as PET/CT, may offer better diagnosis power than the size assessment based on CT. As a non-invasive examination, PET/CT may provide more benefit for evaluating mediastinal node staging of lung cancer.

The ^{18}F-FDG PET is one of the most widely used imaging techniques for detecting and staging tumors [3], which allows physicians to quantify the increased glycolysis of cancer cells [4]. In clinical routine, the standardized uptake value (SUV) is widely used for PET imaging quantification [5–7], which is a simple semi-quantitative index. It is calculated by measuring the activity concentration in the tumor during a scan acquired late (typically 45–60 min) after injection and normalizing for the injected dose and patient weight [8, 9]. However, many factors such as the uptake kinetics, body mass index, or post-injection time can influence the outcome of SUV, as reported for example in lung cancer [10]. Patlak analysis among all kinetic models is usually regarded as a gold standard which presents the ^{18}F-FDG net influx rate constant (i.e., the uptake rate constant, K_i) from a linear fitting of graphical data [11]. It uses the tumor time activity curve (TAC), a tracer kinetic model and plasma glucose levels to derive a more quantitative measure of the influx rate constant of ^{18}F-FDG. As a result, to calculate the Patlak slope, K_i, a dynamic acquisition over the tissue of interest is required. Both a tumor TAC and input function (i.e., the arterial ^{18}F-FDG blood concentration as a function of time) must be measured by a serial blood sampling [12] or from the PET image-derived input function (IDIF) from the dynamic acquisition [13–15].

In this study, we applied the ^{18}F-FDG PET dynamic modeling approach, Patlak analysis, to investigate the imaging quantification of MLN and PT for NSCLC, and to explore the potential of this methodology for differentiating different groups of primary (M0) and metastatic (M1) lung cancers. Furthermore, another aim was to investigate the correlation between SUV and K_i for variety groups.

Material and methods

Patients

Prior to inclusion, all patients were examined by chest CT and no patient had received any therapies. Initially, 76 suspected lung cancer patients indicated by chest CT were included in this study. Dynamic ^{18}F-FDG PET was performed on these 76 suspected lung cancer patients. Then, all these 76 patients underwent CT-guide percutaneous lung puncture biopsy and partial patients received surgical excision and mediastinal MLN dissection without preoperative anti-tumor therapy between June 2017 and May 2019 at our hospital. Fourteen cases were excluded due to lack of pathological validation or the final pathological examination confirmed not to be the diagnosis of NSCLC. Eventually, 62 cases diagnosed NSCLC were included in this study: 37 with newly diagnosed early and locally advanced lung cancer (group M0, i.e., without distant metastases) and 25 with metastatic lung cancer (group M1, i.e., with distant metastases). Grouping was performed by two experienced oncologists, based on the 8th edition of the TNM classification of lung cancer [16]. In these 62 patients, 39 had gene sequencing, in which 21 without EGFR mutation, 9 with exon 19 mutation, and 9 with exon 21 mutation. The process of case inclusion is shown in Fig. 1. The study was approved by the institutional review board of the Fifth Affiliated Hospital, Sun Yat-sen University, and all subjects signed an informed consent form before entry. The clinical trial registration number is NCT03679936 (http://www.clinicaltrials.gov/). All patients in group M0 (19 men and 18 women) and group M1 (14 men and 11 women) were age matched, and their mean age, mean height, and mean body weight (± SD) are summarized in Table 1. No patients had diabetes, severe cardiovascular disease, and other malignant

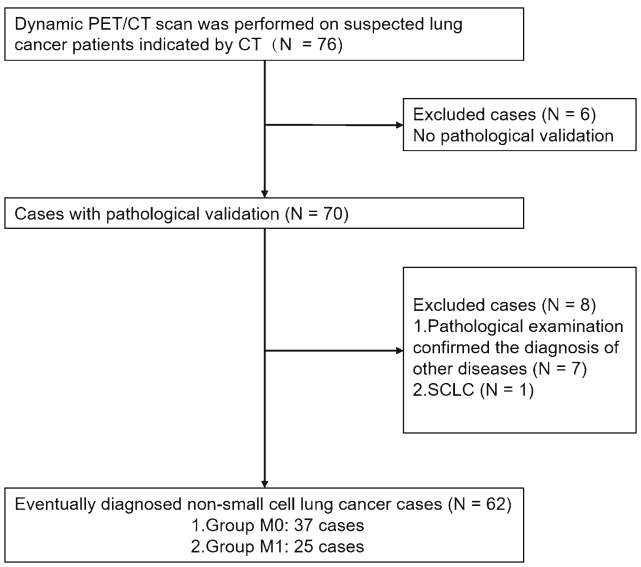

Fig. 1 Flow chart of selection processes of eligible cases

Table 1 Patient characteristics

Category		Group M0 ($n = 37$)	Group M1 ($n = 25$)	p value
Gender	Male	19	14	0.72
	Female	18	11	
Age (mean ± SD) (years)		58 ± 8	56 ± 11	0.26
Height (mean ± SD) (cm)		163.02 ± 9.72	164.61 ± 11.09	0.55
Weight (mean ± SD) (kg)		63.21 ± 13.53	59.94 ± 11.65	0.33
Histopathology (NSCLC)	SCC	7	4	0.93
	AC	25	18	
	Other	5	3	
MLNs		25	25	
EGFR wild type		13	8	0.14
EGFR exon 19 mutation		4	5	
EGFR exon 21 mutation		8	1	

SCC squamous cell carcinoma, *AC* adenocarcinoma, *MLN* metastatic lymph node

diseases. Besides, personal information of all patients was masked by following the standard electronic health record (EHR) process (a common technique used to alter information within a patient's EHR including data encryption, obfuscation, hashing, exclusion, and perturbation) of concealing patient health data to protect patients' sensitive information.

PET data acquisition and reconstruction

All 76 patients fasted for at least 6 h before scans. Patients were prepared according to the published guidelines for quantitative ^{18}F-FDG PET studies [17, 18]. All PET studies were performed on 112-ring digital light guide PET/CT (uMI780, United Imaging, China) over an approximately 30-cm axial field of view. Scans were performed from the apex of lung to the lower margin of liver. Patients were scanned in the supine position with both arms over head. During each scan, firstly a 5-s transmission CT scan (160 mA, 100 kV, pitch 0.9875, rotation time 0.5 s) was performed for subsequent attenuation correction of PET emission data. Secondly, a bolus of ^{18}F-FDG (mean 228 MBq; range 143–327 MBq) was injected intravenously and a dynamic emission scan was started simultaneously. Each dynamic PET study consists of 48 frames acquired in 60 min (18 × 5 s, 6 × 10 s, 5 × 30 s, 5 × 60 s, 8 × 150 s, 6 × 300 s) and was corrected for isotope decay, scattering events, and random coincidence. All emission scans were reconstructed as 150 × 150 matrices. In addition, the acquired data were reconstructed using ordered subsets expectation maximization (OSEM) [19, 20] with 2 iterations and 20 subsets.

PET data analysis

The evaluation of the dynamic PET data was performed using the software of Dynamic Analysis of United Imaging (United Imaging, China). Images were analyzed by two experienced nuclear medicine physicians. The reconstructed PET data was analyzed as follows: (i) definition of volumes of interest (VOIs); (ii) determination of image-derived input function (IDIF) and TAC of different lesions including PT and MLN; (iii) obtaining the K_i through Patlak analysis; (iv) visual and semi-quantitative analysis of static images via SUV.

The Patlak analysis is the most frequently used modeling methods to provide quantitative information for ^{18}F-FDG PET studies. This method requires the plasma TAC as the input function, which theoretically requires arterial blood sampling [12]. Although blood sampling is considered a gold standard because of its high accuracy, it provides challenges and additional risks in routine clinical practice. Subsequent studies have solved the problem by investigating the use of IDIF [14, 15], i.e., the input function can be retrieved from the image data with good accuracy by noninvasive methods [13]. To obtain the IDIF, in each patient, VOIs were drawn manually on early frames, which highlight the arterial blood pool. Small ellipsoid VOIs were drawn on right atrium, left ventricle, and aortic arch [15] in all cases. The regions were small and far from the myocardial wall, in order to minimize spillover and partial volume effects [21]. These input VOIs were then projected onto all 48 frames yielding whole arterial blood TAC, i.e., IDIF (Fig. 2).

To obtain the TAC of different lesions, ellipsoid VOIs were drawn manually over the PTs and MLNs. Regarding MLNs, two individual experienced radiologists examined the suspected lymph nodes on CT for all patients. Only those lymph nodes that both radiologists have confirmed positively were collected for PET analysis. In group M0, 25 sites of MLN were identified based on radiological characteristics (size, shape, margin). In group M1, also 25 sites of the most significant MLN were identified on

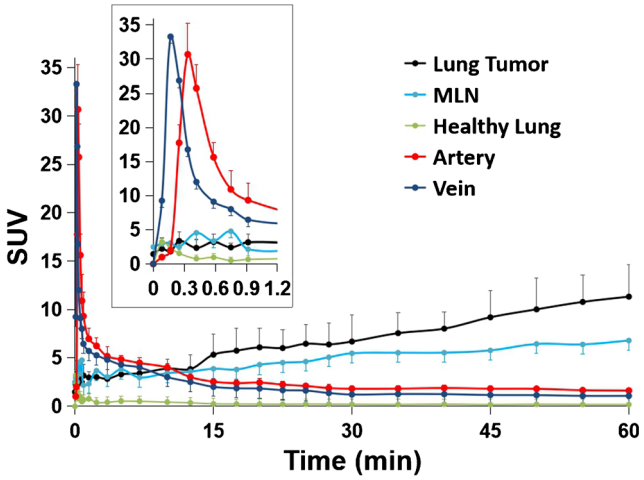

Fig. 2 PET image-derived input function from the dynamic acquisition. Input function (the first 72 s after injection) based on right atrium (blue) and aortic arch (red). Averaged time activity curves (TAC) of lung tumor (blank) and metastatic lymph nodes (MLN, blue), and healthy lung (green) from patients of group M1. The error bars are the standard errors from lung cancer patients of group M1

the condition that for each patient only one most confirmed MLN was chosen based on two radiologists. As a result, the 62 diagnosed NSCLC patients provided a dataset of 62 separate PT sites (37 from group M0; 25 from group M1) and 50 MLN sites (25 from group M0; 25 from group M1). These VOIs were then projected onto all frames of the original reconstructed dynamic study to provide tumors and MLN TACs (Fig. 2).

Patlak analysis was performed using the IDIF and tumor TACs. This model (Fig. 3) assumes unidirectional uptake of ^{18}F-FDG (i.e., $k_4 = 0$), with irreversible trapping in tissue as ^{18}F-FDG-6-PO$_4$, whose details have been described [11]. The influx rate constant (K_i) was calculated by least square method data regression by applying all related TAC data to the Matlab software (Version 2014a, MathWorks Inc., Natick, MA, USA). In brief, the Patlak plot was given by the expression:

$$\frac{C_{tissue}(t)}{Cp(t)} = Ki\frac{\int_0^t Cp(\tau)d\tau}{Cp(t)} + V$$

where the Ki was derived from the slope of graphical analysis whereby the PET measured TAC undergone a transformation. This means that the measured PET activity of certain tissue (C_{tissue} (t) was divided by plasma activity (Cp (t), and plotted at a "normalized time" (τ), integral of input curve from injection divided by instantaneous plasma activity. For systems with irreversible compartments this plot resulted in a straight line after sufficient equilibration time. The Patlak Plot model calculates and displays the transformed measurements as described by the formula above. It allows fitting a regression line within a range defined by the parameters t*. The results were the regression slope and the intercept. There was also an error criterion Max Err. to fit t*. For instance, if Max Err. was set to 10% and the fit box of t* was checked, the model searched the earliest sample so that the deviation between the regression and all measurements was less than 10%. Samples earlier than the t* time were disregarded for regression. Note that t* must be specified in real acquisition time, although the x-axis units were in "normalized time." The corresponding normalized times from our studies were normally applied frame from 30 to 48, where it stands the duration time from 10 to 60 min p.i.

For static analysis, the uptake of FDG on the last frame (at 55–60 min) of dynamic scans was used. The value of SUV within each VOI was selected as below:

$$\text{SUV} = \frac{\text{Radioactivity Concentration in Volum of Interest (MBq/mL)}}{\text{Injected Dose (MBq)/Weight of Patient (g)}} \quad (1)$$

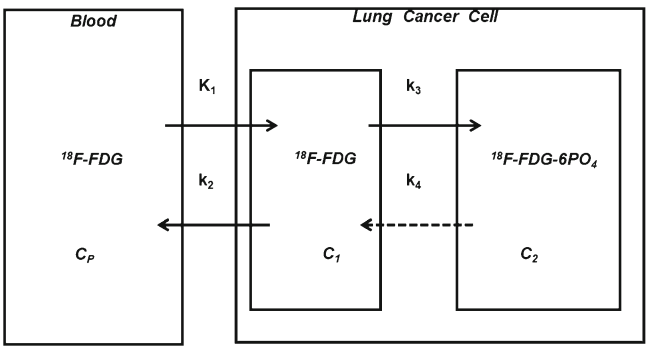

$$\frac{dC_1(t)}{dt} = K_1 C_{input}(t) - (k_2 + k_3)C_1(t) + k_4 C_2(t)$$

$$\frac{dC_2(t)}{dt} = K_3 C_1(t) - k_4 C_2(t)$$

$$\frac{C_{ROI}(t)}{C_P(t)} = K_i \cdot \left(\frac{\int_0^t C_P(\tau)d\tau}{C_P(t)}\right) + V$$

$$K_i = \frac{K_1 \cdot k_3}{k_2 + k_3}$$

Fig. 3 Patlak model for ^{18}F-FDG catabolism. C_P is the activity concentration of ^{18}F-FDG in the blood plasma, and C_1 and C_2 are the concentrations of ^{18}F-FDG and ^{18}F-FDG -6PO$_4$ inside the lung cancer cell. K_1, k_2, k_3, k_4 are rate constants. K_1 is the rate constant from blood to cell; k_2 is the rate constant from cell to blood; k_3 represents the rate constant of ^{18}F-FDG to ^{18}F-FDG-6PO$_4$; notably the rate constant (k_4) of ^{18}F-FDG-6PO$_4$ to ^{18}F-FDG is negligible due to the Patlak analysis assuming unidirectional uptake of ^{18}F-FDG (i.e., $k_4 = 0$). The dynamic model is represented by the above equations. The slope (K_i, influx rate of ^{18}F-FDG) and intercept (V) can be derived from the graphic analysis as described in the method, where the slope K_i equals $K_1K_3/(K_2 + K_3)$

Histological analysis

For patients who had received CT-guide percutaneous lung puncture biopsy or surgery, all punctured or excised tumor and lymph node tissues were fixed in formalin, dehydrated and embedded in paraffin. Five-micrometer sections of each tissue were stained with hematoxylin and eosin (H&E). The H&E slices were evaluated by two experienced pathologists.

Statistics

Mean age, height, and weight were compared using the two-sided Student *t* test, unpaired. A chi-square test was used to compare the sex ratio between the two groups. A normal distribution of the SUV and K_i values in the current study could not be clearly showed; therefore, the statistical evaluation was performed using the descriptive statistics (mean ± SD), scatter plots, non-parametric Mann-Whitney's test (i.e., *U* test), and Kruskal-Wallis test as well as Spearman correlation (GraphPad Prism 6 software; two-tailed; 95% confidence level) [22]. The *p* value was considered statistically significant if $p < 0.05$.

Results

Analysis of data from PTs between group M0 and M1

PT of group M1 had a higher SUV (8.41 ± 0.64) than group M0 (5.23 ± 0.73, Table 2). A significant difference in SUV between two groups was observed ($p < 0.01$, Fig. 4a). This suggested that lesions of PT from static analysis provided significant higher SUV in NSCLC when distant metastases have been already found.

Similarly, values of K_i from PT of group M1 (0.050 ± 0.005 min^{-1}) were higher than group M0 (0.026 ± 0.004 min^{-1}, Table 2). Statistical analysis also showed a significant difference between two groups ($p < 0.001$, Fig. 4b). Consistency between static and dynamic analysis for two groups indicates that both static and dynamic analysis can be used to differentiate status of primary tumors.

Analysis of data from PTs between SCC and AC

For tumors from different histopathology subtype, values of SUV (Fig. 5a) showed obvious difference ($p < 0.05$) between SCC (9.14 ± 1.48) and AC (5.58 ± 0.62, Table 2). In accord with static data, there was also a significant difference of K_i values ($p < 0.05$, Fig. 5b) between SCC (0.052 ± 0.009 min^{-1}) and AC (0.029 ± 0.004 min^{-1}, Table 2).

It is shown in Fig. 5c that SUV values of adenocarcinoma in group M0 (3.48 ± 0.71) were lower than those in group M1 (8.00 ± 0.83, Table 2). Significant statistical difference was found in these two groups ($p < 0.001$). Same as static results, adenocarcinoma in group M0 has a lower K_i value (0.017 ± 0.004 min^{-1}) than in group M1 (0.046 ± 0.006 min^{-1}, Table 2). For statistical analysis, two groups showed a significant difference ($p < 0.001$, Fig. 5d).

Analysis of data from MLNs between group M0 and M1

When it comes to MLNs, SUV values of group M1 (5.57 ± 0.59) were slightly higher than that of group M0 (4.22 ± 0.49, Table 2). No significant difference between two groups was found ($p > 0.05$, Fig. 4c). However, the result of dynamic analysis from MLNs was in sharp contrast to the finding of static analysis. Values of K_i from group M1 (0.033 ± 0.005 min^{-1}) were much higher than group M0 (0.016 ± 0.003 min^{-1}, Table 2). Statistical analysis showed significant difference between two groups ($p < 0.01$, Fig. 4d).

Representative examples of MLN in group M0 and group M1 are illustrated in Fig. 6a–c. Figure 6 a and b are the PET/CT images of MLN of a patient without and with distant metastases, respectively. As is shown in Fig. 6 a and b, a high ^{18}F-FDG accumulation of MLN (red arrow)

Table 2 Values of SUV and K_i from different groups

Groups	SUV (mean ± SD)	*p* value*	K_i (min^{-1}) (mean ± SD)	*p* value*
PTs in group M0 ($n = 37$)	5.23 ± 0.73	< 0.01	0.026 ± 0.004	< 0.001
PTs in group M1 ($n = 25$)	8.41 ± 0.64		0.050 ± 0.005	
MLNs in group M0 ($n = 25$)	4.22 ± 0.49	> 0.05	0.016 ± 0.003	< 0.01
MLNs in group M1 ($n = 25$)	5.57 ± 0.59		0.033 ± 0.005	
SCC ($n = 11$)	9.14 ± 1.48	< 0.05	0.052 ± 0.009	< 0.05
AC ($n = 43$)	5.58 ± 0.62		0.029 ± 0.004	
AC in group M0 ($n = 25$)	3.84 ± 0.71	< 0.001	0.017 ± 0.004	< 0.001
AC in Group M1 ($n = 18$)	8.00 ± 0.83		0.046 ± 0.006	

**U*-test

PT primary tumor, *MLN* metastatic lymph node, *SCC* squamous cell carcinoma, *AC* adenocarcinoma

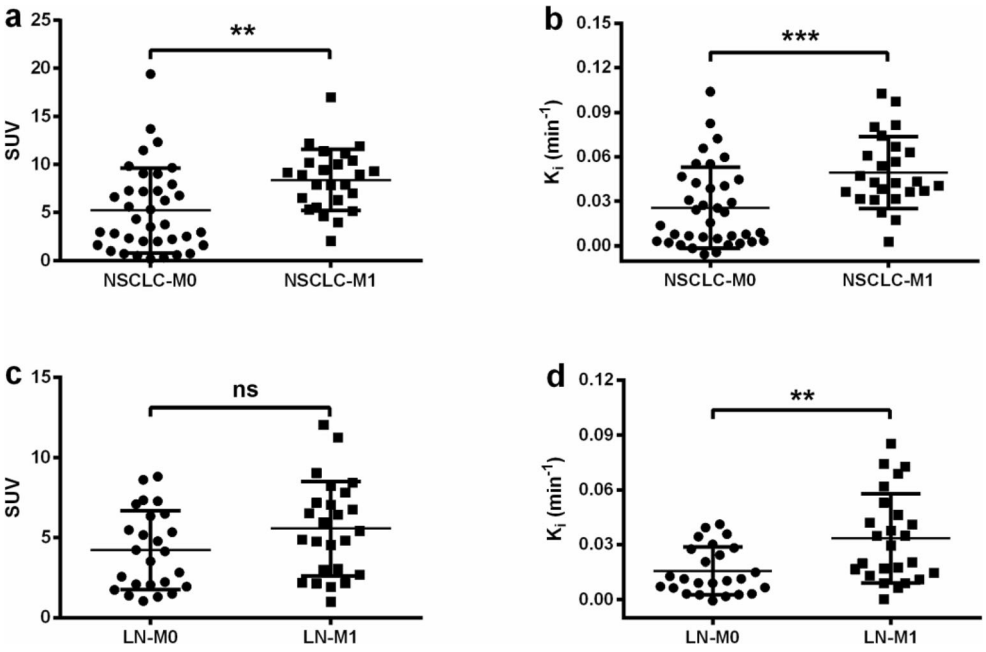

Fig. 4 K_i^{MLN} of metastatic lymph nodes (MLNs) showed more sensitivity than the static analysis SUV^{MLN} to detect MLNs in NSCLC, although both methods were sensitive for primary tumors (PTs). **a**, **b** Comparison of SUV (**a**) and K_i (**b**) from PTs between group M0 and group M1; **c**, **d** comparison of SUV (**c**) and K_i (**d**) from MLNs between group M0 and group M1; $*p < 0.05$, $**p < 0.01$, $***p < 0.001$; ns, not significant

can be observed with corresponding SUV values as 8.62 and 8.24, respectively. Therefore, from the static data, it was hard to distinguish distinct difference between M0 and M1. However, K_i value of lesion in Fig. 6 a and b was 0.03 min^{-1} and 0.07 min^{-1} (Fig. 6c), respectively. MLN in metastatic NSCLC was prone to have a higher value of K_i than in non-metastatic NSCLC.

Encouraged by the higher K_i values of MLN in group M1, we questioned whether this method can differ the malignant lymph nodes from the benign lymph nodes. Representative cases are shown in Fig. 7. As is shown in Fig. 7 a and b, according to lymph node size, shape, and uptake on PET/CT, they appeared to be the same and was difficult to identify their metastatic status (both were prone to be benign according to clinical experience of two physicians). Interestingly, both of two patients received surgical resection and systematic nodal dissection. Postoperative pathology (Fig. 7c–d) showed lymph node in Fig. 7a was benign, malignant in Fig. 7b. K_i value of lymph node (Fig. 7e) in Fig. 7a is 0.010 min^{-1}, whereas 0.02 min^{-1} in Fig. 7b. The pathological confirmation

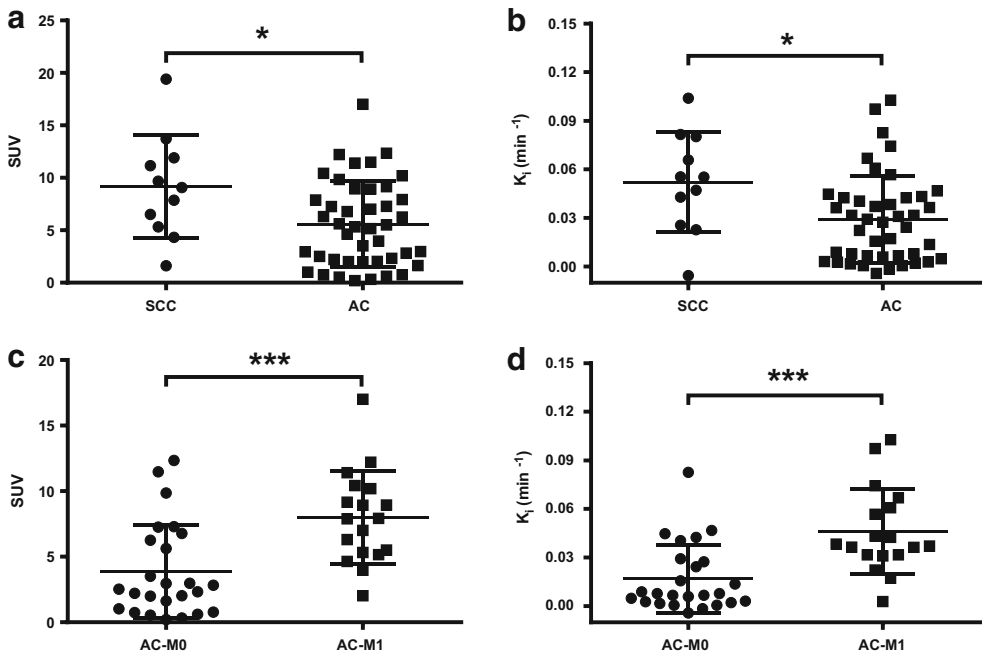

Fig. 5 Both SUV^{PT} and K_i^{PT} showed significant high values in squamous cell carcinoma than adenocarcinoma. **a**, **b** Comparison of SUV (**a**) and K_i (**b**) from primary tumors between squamous cell carcinoma (SCC) and adenocarcinoma (AC); **c**, **d** comparison of SUV (**c**) and K_i (**d**) from primary tumors between AC in group M0 and group M1; $*p < 0.05$, $**p < 0.01$, $***p < 0.001$; ns, not significant

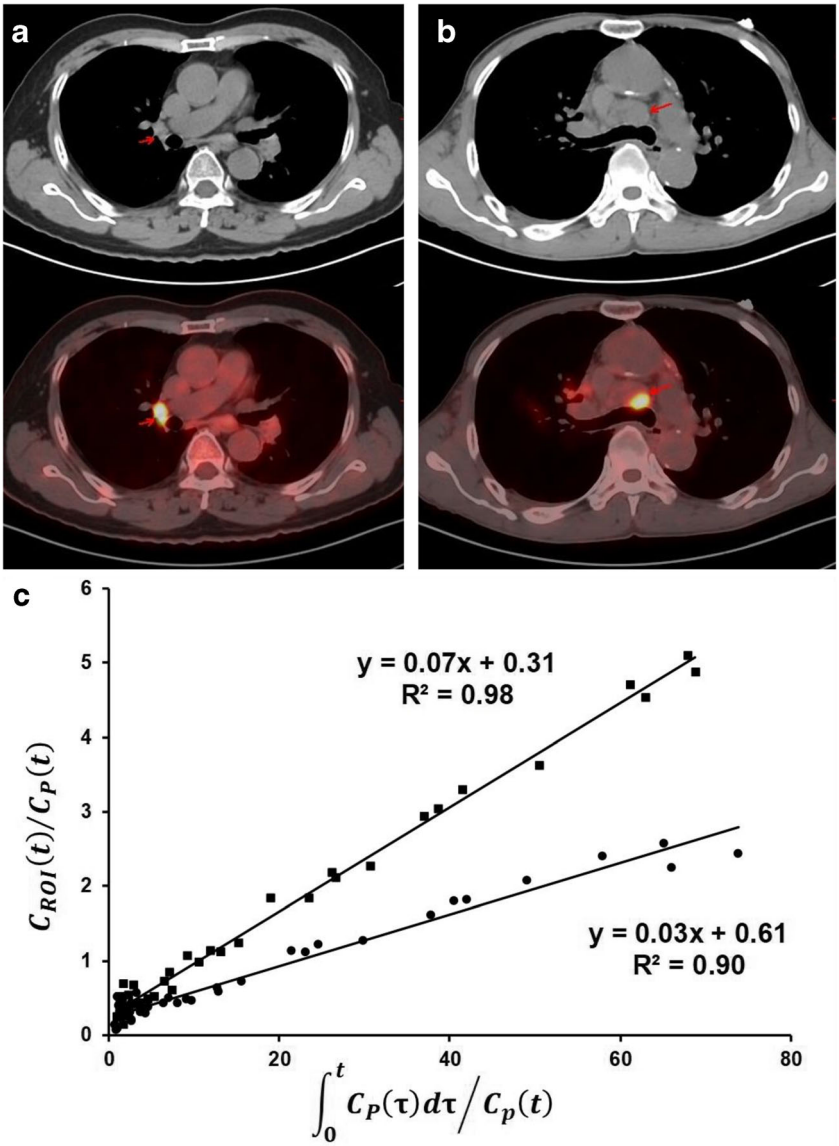

Fig. 6 Representative PET/CT images of metastatic lymph node (MLN). Examples of MLN (red arrows) from group M0 (**a**) and group M1 (**b**), and Patlak plots (**c**) of the lymph nodes in **a** (circle) and **b** (square). Noting a higher slope of MLN in group M1 than in group M0, indicating a higher K_i in lymph node

further validated a higher value of the ^{18}F-FDG influx rate constant of MLN from the dynamic data modeling.

Analysis of data from PTs of different EGFR mutations

We compared SUV and K_i (Online Resource 1) values from EGFR wild type, exon 19 mutation and exon 21 mutation (Kruskal-Wallis test). No significant difference was found between different groups either from dynamic modeling (K_i^{PT}) or statics analysis (SUV^{PT}).

Analysis of correlation between SUV and K_i from different groups

The correlation between SUV and K_i of different groups was investigated. As is shown in Table 3, SUV and K_i of SCC showed a strong correlation ($r = 0.93$). SUV and K_i of PTs in group M0 ($r = 0.88$), adenocarcinoma ($r = 0.87$), and adenocarcinoma in group M0 ($r = 0.86$) showed a moderate correlation. A weak correlation between SUV and K_i of PTs in group M1 ($r = 0.77$), MLNs in group M1 ($r = 0.77$), and adenocarcinoma in group M1 ($r = 0.77$) was found. A poor correlation ($r = 0.77$, 95% confidence interval 0.53 to 0.90) between SUV and K_i of MLNs in group M1 was found.

Discussion

To our knowledge, our study provided the first quantitative assessment, Patlak analysis, of PTs and MLNs status, such as metastasis status, histological subtype, and EGFR mutation status of NSCLC using dynamic ^{18}F-FDG PET/CT.

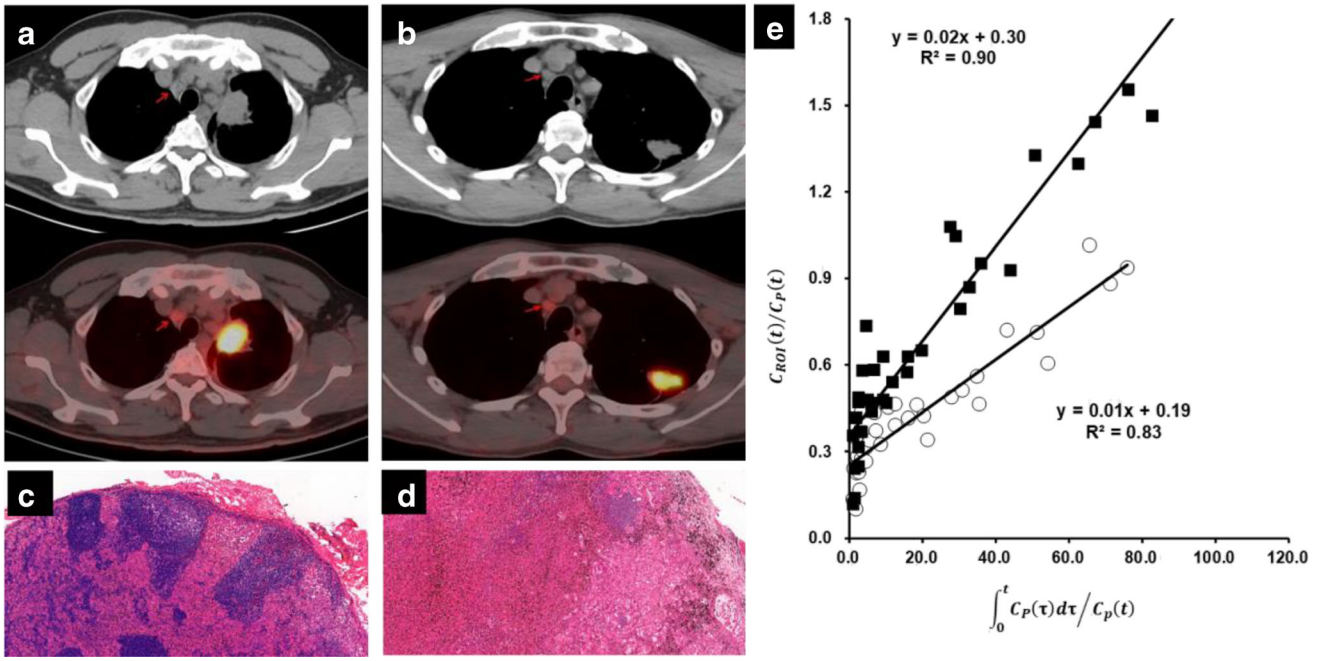

Fig. 7 Representative PET/CT images of benign lymph node and malignant lymph node. Images of benign lymph node (**a**) and malignant lymph node (**b**) with similar SUV (1.95 and 2.07, respectively). The HE staining (× 40) of lymph nodes: benign lymph node (**c** from **a**) shows normal lymph node structure, while malignant lymph node (**d** from **b**) shows scattered cancer nests infiltrate into lymphoid tissue. **e** Patlak plots of the lymph nodes from **a** (benign LN, circle, $K_i = 0.01$) and **b** (malignant LN, square, $K_i = 0.02$)

Nevertheless, previous studies focused on static scanning mostly.

Our results suggested that the ^{18}F-FDG PET dynamic modeling was a reliable approach to identify more metastatic lymph nodes than the conventional static analysis, and its outcomes had strong correlations with histological subtypes.

^{18}F-FDG accumulation is related to many factors, such as the presence of necrosis, vascular density, HIF-1 α (hypoxia-inducible factor-1 α), activity of glucose transporters (GLUTs), and glycolytic enzymes (i.e., hexokinases, HKs).

Table 3 Correlation coefficient (Spearman *r*) between SUV and K_i from different groups

SUV vs K_i	*r*	95% confidence interval	*p* value
PTs in group M0	0.88	0.78 to 0.94	< 0.0001
PTs in group M1	0.76	0.51 to 0.89	< 0.0001
MLNs in group M0	0.81	0.61 to 0.92	< 0.0001
MLNs in group M1	0.77	0.53 to 0.90	< 0.0001
SCC	0.93	0.73 to 0.98	0.0001
AC	0.87	0.77 to 0.93	< 0.0001
AC in group M0	0.86	0.70 to 0.94	< 0.0001
AC in group M1	0.77	0.46 to 0.91	0.0002

PT primary tumor, *MLN* metastatic lymph node, *SCC* squamous cell carcinoma, *AC* adenocarcinoma

Baardwijk et al. [23] indicated that NSCLC with a high SUV expressed a higher proportion HIF-1 α and GLUT-1 than tumors with a low SUV and hypoxia was associated with a higher uptake of FDG. Chung et al. [24] and Higashi et al. [25] also showed that FDG uptake generally correlated with GLUT-1 expression in NSCLC. Berkel et al. [26] suggested that increased accumulation of ^{18}F-FDG was largely determined by increased HK activity. In group M0, most PTs were small with a low uptake of FDG; moreover, some ground glass opacity (GGO) with few solid components had little uptake. However, in group M1, most PTs were larger with obvious uptake of FDG and spread to other organs such as lung, liver, adrenal gland, and bone. The reason why most PTs of group M1 had higher SUV and K_i values than that of group M0 may be hypoxia and a higher HIF-1 α, GLUT-1, and HK expression. Meanwhile, we also noted that some tumors grew very large without distant metastasis while some tumors were small with distant metastasis; as a result, it could be seen sometimes that PTs of group M0 had higher SUV and K_i values than PTs of group M1. We speculated that tumor metastasis was not only related to tumor size but also related to tumor pathological subtypes, differentiation, and grades. In order to investigate the influence of pathological subtypes on SUV and K_i, we studied the most common pathological subtype in NSCLC, i.e., SCC and AC. Being consistent with other study, Geus-Oei et al. [27] also showed that FDG uptake was significantly higher in SCC compared with AC.

Simultaneously, they illustrated that tumor cell differentiation in combination with overexpression of GLUT-1 and GLUT-3 determines the extent of FDG accumulation. We speculated this may be the same reason why SCC had a higher SUV and K_i value than AC.

It is noteworthy that no significant difference of MLNs between two groups was found according to SUV. Interestingly, K_i value of lymph nodes in group M1 was higher than that in group M0. A limitation of this comparison was the lack of histological confirmation for all lymph nodes. In clinical practice, it is not possible to confirm by histology every indicative lymph node, especially for patient who has not undergone surgery. In fact, only the correlation to other imaging modalities, like CT and MRI, and the patient's clinical outcome serve as a reference. In this study, all MLNs were identified by two experienced physicians.

Freedman et al. [21] showed that different conclusions could be reached regarding tumor follow-up depending on whether SUV or Patlak analysis was used. Weber et al. [28] indicated that the principal sources of variability in measurement of SUV and Patlak K_i were methodological issues such as accuracy of placement of VOIs. While accurate placement of VOIs may affect the absolute values of SUV and Patlak K_i, it will have no impact on our comparison of these two indices, since the same VOIs and the identical FDG data set were used for both.

It is certain that the two methods do not measure the same quantity. Findings of others [29–31] indicated that SUV correlates well but not perfectly with glucose metabolic rate. FDG trapped in the tumor cell cannot metabolize further after phosphorylation by hexokinase [32]. There are three main differences between SUV and the Patlak K_i [21]. Firstly, SUV measures the total activity in the tumor including both metabolized (e.g., phosphorylated) FDG and unmetabolized (e.g., unphosphorylated) FDG in the blood, intracellular spaces, or cell. Patlak analysis separates these two components out—the Patlak slope is determined only by phosphorylated FDG. Secondly, SUV often depends strongly on how long after injection the static scan is acquired. Patlak slope avoids this time dependence because it is a measure of rate of uptake rather than uptake at a specific time [21]. Often the tumor TACs are still rising even at 60 min [33, 34]. Unless the tumor TAC has reached a plateau, this will cause errors in SUV measured at a fixed time post injection. Thirdly, Patlak slope uses the integral under the arterial input function for normalization. SUV approximates this integral by the injected dose divided by the body weight and may not always accurately reflect tracer metabolism [5, 7, 21]. The three differences make it that K_i value of MLNs provides not the same information than SUV. In addition, tumors with low ^{18}F-FDG uptake, having a relatively high fraction of free FDG, may show larger discrepancies between SUV and Patlak analysis [21, 34, 35].

As for the comparison of PTs from EGFR wild type and different mutations, no significant difference was found between different groups. Sun et al. [36] found that ^{18}F-FDG PET/CT showed high tumor uptake in all NSCLC patient groups, with no apparent visual difference among patients carrying different EGFR mutation status. Our static analysis results were in accordance with theirs. Differently, they found ^{18}F-MPG successfully delineated EGFR-activating mutant tumors, showing visually appreciable higher contrast than EGFR wild-type tumors. Nevertheless, Choi et al. [37] found that the SUV tended to be higher in wild-type than mutant tumors, but was not significantly different. The SUV was significantly lower in patients with exon 19 mutation than in those with either exon 21 mutation or wild type. But Huang et al. [38] reported that the ^{18}F-FDG uptake was significantly higher in EGFR-mutant than wild-type lung adenocarcinoma patients. The reason for the difference between various studies may be the inconsistent sample size and heterogeneity of population. In comparison, as far as we know, we first applied dynamic model methods to investigate the difference of various mutation status of PTs of NSCLC although no significant difference was found between different groups.

As for the correlation between SUV and K_i from different groups, it is definitive that SUV correlates with K_i. Besides, we found that the correlation of SUV with K_i was lower for AC than for SCC; the correlation of SUV with K_i for PTs was lower in group M1 than in group M0; the correlation of SUV with K_i for MLNs was lower in group M0 than in group M1. There is no plausible explanation for the observed effects at present, whereas a relatively poor correlation between SUV and K_i of MLNs may be a reasonable explanation of the difference between MLNs in group M0 and M1 indicated by K_i.

From our study, static analysis results were correlated well with dynamic analysis results in most cases for PTs. However, Patlak analysis is rarely used in clinical routine because of the time-consuming, full dynamic acquisition protocol they involve. In clinical practice, static analysis requires only 1 late image acquisition, so SUV is recommended first. But for some small lymph node with low uptake, according to static PET/CT, it is difficult for physicians to give a definite diagnosis; thus, dynamic PET/CT may provide us more metastatic information.

Our study is exploratory and pilot research. Results from this analysis should be interpreted with care, because the number of patients in each group was not large enough. Moreover, a dynamic scan is also more sensitive to patient motion which could affect the accuracy of Patlak analysis. Thirdly, the current study did not use respiratory gating, and in the case of lesions in the lower lobes of lung, respiratory artifacts may very likely affect the outcomes of Patlak analysis. Despite the small sample size, however, the finding of such large discrepancies in statistical analysis of MLNs is a strong evidence that the discrepancies may be important. At least in our study,

values of K_i from Patlak analysis can provide more robust information about metastatic lymph node than SUV.

Conclusion

Both SUV and K_i were potential methods to evaluate primary tumor status. However, SUV failed to detect any difference of MLNs between group M0 and group M1, while the K_i values succeed in doing so. Our study provided the evidence that the K_i values were more sensitive than the regular SUV to identify the earlier lymph node, in which the conventional static PET may not yet indicate a positive result. This suggested that for some suspected lymph nodes that SUV cannot identify exactly, K_i may be helpful. Currently ongoing further studies are warranted to confirm the consistency of the results. These clinical trials will expand the kinetics modeling quantification for other clinical applications including lung cancer (NCT03679936), liver cancer (NCT03636607), esophageal squamous cell carcinoma (NCT03657914), and papillary thyroid cancer (NCT03830242).

Author contributions All authors contributed to the study conception and design; the final analysis and writing of the manuscript.

Funding information This work was funded by the National Key R&D Program of China (2018YFC0910601), the National Natural Science Foundation of China (No.81871382), and Starting Fund from Sun Yat-sen University Fifth Affiliated Hospital.

Data availability The datasets used and analyzed during the current study are available from the corresponding author on reasonable request.

Compliance with ethical standards

Conflict of interest The authors declare that they have no conflict of interest.

Ethical approval All procedures performed in studies involving human participants were in accordance with the ethical standards of the institutional research committee and with the 1964 Helsinki declaration and its later amendments or comparable ethical standards.

Informed consent Informed consent was obtained from all individual participants included in the study.

References

1. May M. Statistics: attacking an epidemic. Nature. 2014;509:S50–1. https://doi.org/10.1038/509S50a.
2. Lortet-Tieulent J, Soerjomataram I, Ferlay J, Rutherford M, Weiderpass E, Bray F. International trends in lung cancer incidence by histological subtype: adenocarcinoma stabilizing in men but still increasing in women. Lung Cancer (Amsterdam, Netherlands). 2014;84:13–22. https://doi.org/10.1016/j.lungcan.2014.01.009.
3. Strauss LG. Fluorine-18 deoxyglucose and false-positive results: a major problem in the diagnostics of oncological patients. Eur J Nucl Med. 1996;23:1409–15.
4. Som P, Atkins HL, Bandoypadhyay D, Fowler JS, MacGregor RR, Matsui K, et al. A fluorinated glucose analog, 2-fluoro-2-deoxy-D-glucose (F-18): nontoxic tracer for rapid tumor detection. J Nucl Med : official publication, Society of Nuclear Medicine. 1980;21:670–5.
5. Hamberg LM, Hunter GJ, Alpert NM, Choi NC, Babich JW, Fischman AJ. The dose uptake ratio as an index of glucose metabolism: useful parameter or oversimplification? J Nucl Med : official publication, Society of Nuclear Medicine. 1994;35:1308–12.
6. Huang SC. Anatomy of SUV. Standardized uptake value. Nucl Med Biol. 2000;27:643–6.
7. Keyes JW Jr. SUV: standard uptake or silly useless value? J Nucl Med : official publication, Society of Nuclear Medicine. 1995;36:1836–9.
8. Sugawara Y, Zasadny KR, Neuhoff AW, Wahl RL. Reevaluation of the standardized uptake value for FDG: variations with body weight and methods for correction. Radiology. 1999;213:521–5. https://doi.org/10.1148/radiology.213.2.r99nv37521.
9. Zasadny KR, Wahl RL. Standardized uptake values of normal tissues at PET with 2-[fluorine-18]-fluoro-2-deoxy-D-glucose: variations with body weight and a method for correction. Radiology. 1993;189:847–50. https://doi.org/10.1148/radiology.189.3.8234714.
10. Laffon E, de Clermont H, Begueret H, Vernejoux JM, Thumerel M, Marthan R, et al. Assessment of dual-time-point 18F-FDG-PET imaging for pulmonary lesions. Nucl Med Commun. 2009;30:455–61. https://doi.org/10.1097/MNM.0b013e32832bdcac.
11. Patlak CS, Blasberg RG, Fenstermacher JD. Graphical evaluation of blood-to-brain transfer constants from multiple-time uptake data. J Cereb Blood Flow Metab : official journal of the International Society of Cerebral Blood Flow and Metabolism. 1983;3:1–7. https://doi.org/10.1038/jcbfm.1983.1.
12. Phelps ME, Huang SC, Hoffman EJ, Selin C, Sokoloff L, Kuhl DE. Tomographic measurement of local cerebral glucose metabolic rate in humans with (F-18)2-fluoro-2-deoxy-D-glucose: validation of method. Ann Neurol. 1979;6:371–88. https://doi.org/10.1002/ana.410060502.
13. Gambhir SS, Schwaiger M, Huang SC, Krivokapich J, Schelbert HR, Nienaber CA, et al. Simple noninvasive quantification method for measuring myocardial glucose utilization in humans employing positron emission tomography and fluorine-18 deoxyglucose. J Nucl Med : official publication, Society of Nuclear Medicine. 1989;30:359–66.
14. Chen K, Bandy D, Reiman E, Huang SC, Lawson M, Feng D, et al. Noninvasive quantification of the cerebral metabolic rate for glucose using positron emission tomography, 18F-fluoro-2-deoxyglucose, the Patlak method, and an image-derived input function. J Cereb Blood Flow Metab : official journal of the International Society of Cerebral Blood Flow and Metabolism. 1998;18:716–23. https://doi.org/10.1097/00004647-199807000-00002.
15. van der Weerdt AP, Klein LJ, Boellaard R, Visser CA, Visser FC, Lammertsma AA. Image-derived input functions for determination of MRGlu in cardiac (18)F-FDG PET scans. J Nucl Med : official publication, Society of Nuclear Medicine. 2001;42:1622–9.
16. Detterbeck FC, Boffa DJ, Kim AW, Tanoue LT. The eighth edition lung cancer stage classification. Chest. 2017;151:193–203. https://doi.org/10.1016/j.chest.2016.10.010.
17. Boellaard R. Standards for PET image acquisition and quantitative data analysis. J Nucl Med : official publication, Society of Nuclear Medicine. 2009;50(Suppl 1):11s–20s. https://doi.org/10.2967/jnumed.108.057182.

18. Boellaard R, Oyen WJ, Hoekstra CJ, Hoekstra OS, Visser EP, Willemsen AT, et al. The Netherlands protocol for standardisation and quantification of FDG whole body PET studies in multi-centre trials. Eur J Nucl Med Mol Imaging. 2008;35:2320–33. https://doi.org/10.1007/s00259-008-0874-2.
19. Boellaard R, van Lingen A, Lammertsma AA. Experimental and clinical evaluation of iterative reconstruction (OSEM) in dynamic PET: quantitative characteristics and effects on kinetic modeling. J Nucl Med : official publication, Society of Nuclear Medicine. 2001;42:808–17.
20. Hudson HM, Larkin RS. Accelerated image reconstruction using ordered subsets of projection data. IEEE Trans Med Imaging. 1994;13:601–9. https://doi.org/10.1109/42.363108.
21. Freedman NM, Sundaram SK, Kurdziel K, Carrasquillo JA, Whatley M, Carson JM, et al. Comparison of SUV and Patlak slope for monitoring of cancer therapy using serial PET scans. Eur J Nucl Med Mol Imaging. 2003;30:46–53. https://doi.org/10.1007/s00259-002-0981-4.
22. Vieira S, Corrente JE. Statistical methods for assessing agreement between double readings of clinical measurements. J Appl Oral Sci : revista FOB. 2011;19:488–92.
23. van Baardwijk A, Dooms C, van Suylen RJ, Verbeken E, Hochstenbag M, Dehing-Oberije C, et al. The maximum uptake of (18)F-deoxyglucose on positron emission tomography scan correlates with survival, hypoxia inducible factor-1alpha and GLUT-1 in non-small cell lung cancer. Eur J Cancer (Oxford, England : 1990). 2007;43:1392–8. https://doi.org/10.1016/j.ejca.2007.03.027.
24. Chung JK, Lee YJ, Kim SK, Jeong JM, Lee DS, Lee MC. Comparison of [18F]fluorodeoxyglucose uptake with glucose transporter-1 expression and proliferation rate in human glioma and non-small-cell lung cancer. Nucl Med Commun. 2004;25:11–7.
25. Higashi K, Ueda Y, Sakurai A, Mingwang X, Xu L, Murakami M, et al. Correlation of Glut-1 glucose transporter expression with [(18)F]FDG uptake in non-small cell lung cancer. Eur J Nucl Med. 2000;27:1778–85. https://doi.org/10.1007/s002590000367.
26. van Berkel A, Vriens D, Visser EP, Janssen MJR, Gotthardt M, Hermus A, et al. Metabolic subtyping of pheochromocytoma and paraganglioma by (18)F-FDG pharmacokinetics using dynamic PET/CT scanning. J Nucl Med : official publication, Society of Nuclear Medicine. 2019;60:745–51. https://doi.org/10.2967/jnumed.118.216796.
27. de Geus-Oei LF, van Krieken JH, Aliredjo RP, Krabbe PF, Frielink C, Verhagen AF, et al. Biological correlates of FDG uptake in non-small cell lung cancer. Lung Cancer (Amsterdam, Netherlands). 2007;55:79–87. https://doi.org/10.1016/j.lungcan.2006.08.018.
28. Weber WA, Ziegler SI, Thodtmann R, Hanauske AR, Schwaiger M. Reproducibility of metabolic measurements in malignant tumors using FDG PET. J Nucl Med : official publication, Society of Nuclear Medicine. 1999;40:1771–7.
29. Minn H, Leskinen-Kallio S, Lindholm P, Bergman J, Ruotsalainen U, Teras M, et al. [18F]fluorodeoxyglucose uptake in tumors: kinetic vs. steady-state methods with reference to plasma insulin. J Comput Assist Tomogr. 1993;17:115–23.
30. Minn H, Zasadny KR, Quint LE, Wahl RL. Lung cancer: reproducibility of quantitative measurements for evaluating 2-[F-18]-fluoro-2-deoxy-D-glucose uptake at PET. Radiology. 1995;196:167–73. https://doi.org/10.1148/radiology.196.1.7784562.
31. Lodge MA, Lucas JD, Marsden PK, Cronin BF, O'Doherty MJ, Smith MA. A PET study of 18FDG uptake in soft tissue masses. Eur J Nucl Med. 1999;26:22–30.
32. Gallagher BM, Fowler JS, Gutterson NI, MacGregor RR, Wan CN, Wolf AP. Metabolic trapping as a principle of oradiopharmaceutical design: some factors resposible for the biodistribution of [18F] 2-deoxy-2-fluoro-D-glucose. J Nucl Med : official publication, Society of Nuclear Medicine. 1978;19:1154–61.
33. Hoekstra CJ, Paglianiti I, Hoekstra OS, Smit EF, Postmus PE, Teule GJ, et al. Monitoring response to therapy in cancer using [18F]-2-fluoro-2-deoxy-D-glucose and positron emission tomography: an overview of different analytical methods. Eur J Nucl Med. 2000;27:731–43.
34. Sundaram SK, Freedman NM, Carrasquillo JA, Carson JM, Whatley M, Libutti SK, et al. Simplified kinetic analysis of tumor 18F-FDG uptake: a dynamic approach. J Nucl Med : official publication, Society of Nuclear Medicine. 2004;45:1328–33.
35. McDermott GM, Welch A, Staff RT, Gilbert FJ, Schweiger L, Semple SI, et al. Monitoring primary breast cancer throughout chemotherapy using FDG-PET. Breast Cancer Res Treat. 2007;102:75–84. https://doi.org/10.1007/s10549-006-9316-7.
36. Sun X, Xiao Z, Chen G, Han Z, Liu Y, Zhang C, et al. A PET imaging approach for determining EGFR mutation status for improved lung cancer patient management. Sci Transl Med. 2018;10. https://doi.org/10.1126/scitranslmed.aan8840.
37. Choi YJ, Cho BC, Jeong YH, Seo HJ, Kim HJ, Cho A, et al. Correlation between (18)f-fluorodeoxyglucose uptake and epidermal growth factor receptor mutations in advanced lung cancer. Nucl Med Mol Imaging. 2012;46:169–75. https://doi.org/10.1007/s13139-012-0142-z.
38. Huang CT, Yen RF, Cheng MF, Hsu YC, Wei PF, Tsai YJ, et al. Correlation of F-18 fluorodeoxyglucose-positron emission tomography maximal standardized uptake value and EGFR mutations in advanced lung adenocarcinoma. Medical Oncology (Northwood, London, England). 2010;27:9–15. https://doi.org/10.1007/s12032-008-9160-1.